On the onset of convective instabilities in cylindrical cavities heated from below. II. Effect of a magnetic field

R. Touihri,[a] H. Ben Hadid, and D. Henry
Laboratoire de Mécanique des Fluides et d'Acoustique—UMR CNRS 5509, Ecole Centrale de Lyon/Université Claude Bernard-Lyon 1, ECL, BP 163, 69131 Ecully Cedex, France

(Received 12 August 1998; accepted 30 March 1999)

The effect of a constant and uniform magnetic field on electrically conducting liquid-metal flow, in cylindrical cavities heated from below, is numerically analyzed by using a spectral element method to solve the three-dimensional Navier–Stokes and Ohm equations. The cavity is characterized by its aspect ratio defined as $A=H/D$. The lateral surfaces are adiabatic and all the boundaries are electrically insulating. The flow with a vertical magnetic field has the same symmetries as that without a magnetic field, so that similar convective modes ($m=0$, $m=1$, and $m=2$) occur, but they are not equally stabilized. Here m is the azimuthal wave number. For $A=0.5$, for sufficiently large values of the Hartmann number Ha, the mode $m=2$ becomes the critical mode in place of $m=0$. The horizontal magnetic field breaks some symmetries of the flow. The axisymmetric mode disappears giving an asymmetric mode $m=02$, i.e., a combination of the $m=0$ and $m=2$ modes, whereas the asymmetric modes ($m=1$ and $m=2$), which were invariant by azimuthal rotation without a magnetic field, now have two possible orientations, either parallel or perpendicular to the applied magnetic field $\boldsymbol{B}$. These five modes are differently stabilized, weakly if the axis of the rolls is parallel to $\boldsymbol{B}$ and strongly if the axis is perpendicular. Beyond the primary thresholds, the secondary bifurcation, found in the pure thermal case for $A=0.5$, becomes an imperfect bifurcation consisting of two disconnected branches. © *1999 American Institute of Physics.* [S1070-6631(99)02007-3]

I. INTRODUCTION

In some material processing such as crystal growth, a magnetic field is often used to control the liquid flows. Its action will lead to the braking of the flow or to the damping of the convective instabilities. In crystal growth, the control of the flow in the melt will help to improve the quality of the crystal. It is then interesting to understand more precisely the effects of a magnetic field on convective instabilities.

The effect of a constant magnetic field on the electrically conducting liquid-metal flows in heated cavities has been mainly studied for the lateral heating corresponding to horizontal Bridgman crystal growth configurations. BenHadid *et al.*[1] and BenHadid and Henry[2,3] investigated numerically the case of parallelepipedic or cylindrical cavities. Different magnetic field orientations have been considered, as well as different situations in the parallelepipedic case, namely buoyancy-driven convection, in a confined cavity or in a cavity with a stress-free surface at the top boundary, and thermocapillary-driven convection in a cavity where the upper boundary is subjected to a surface tension variation. For long cavities (horizontal length/vertical height$=4$), the magnetic damping is found to be more effective with a vertical field, but this conclusion depends strongly on the characteristics of the configurations: cross-section shape, driving force, and boundary conditions. The behaviors are, in fact, governed by the electric current distribution.

The influence of the cross-section shape on the magnetic damping in the case of long horizontal cavities has been studied analytically by Alboussière *et al.*[4] It has been shown that with electrically insulated walls, the magnetically damped convective velocity varies as Ha^{-2} (Ha is the Hartmann number) when the cross section has an horizontal plane of symmetry, and Ha^{-1} for nonsymmetrical shapes. When the walls are perfectly conducting, the damped velocity always varies as Ha^{-2}. Recently, Alboussière *et al.*[5] made an asymptotic analysis, showing the effect of the symmetries and the electrically boundary conditions on the flows of electrically conducting fluids, under a strong and possibly nonuniform magnetic field. Finally, the stability of such flows has been investigated by Bojarevics[6] assuming the existence of a two-dimensional solution in the rectangular cross section.

The influence of a vertical magnetic field on convection arising in a fluid layer heated from below has been studied by Chandrasekhar.[7] This linear analysis shows that the primary thresholds vary as Ha^2 and the wave numbers decrease as $\mathrm{Ha}^{-1/3}$.

A further work performed by Baumgartl and Müller[8] compared three magnetohydrodynamic models of different complexity to calculate the effect of magnetic damping on fluid flow in a cylindrical cavity heated from below. They showed that the first approximation (MHD1) is not able to reproduce three-dimensional or time-dependent magnetohydrodynamic phenomena. For steady-state or slowly varying flow the second approximation (MHD2) seems to be suffi-

[a]Electronic mail: touihri@mecaflu.ec-lyon.fr

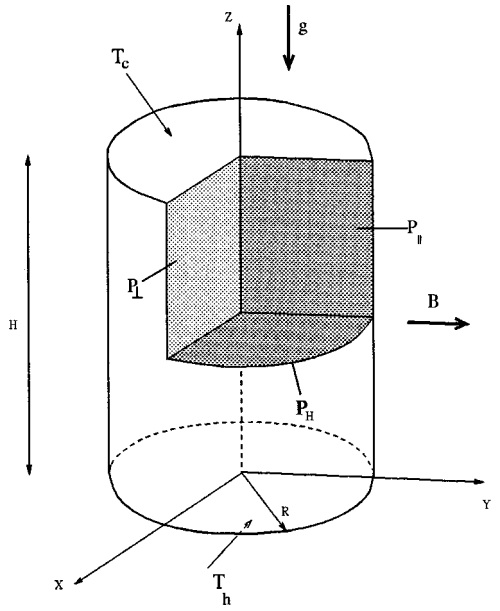

FIG. 1. Cavity configuration with horizontal magnetic field.

ciently accurate. When the time dependence of the induced magnetic field cannot be neglected, e.g., with turbulent flows, their most complex approximation (MHD3) should be used. Recently Mössner[9] studied the damping of the flow in a laterally confined fluid layer heated from below, showing the increase of the number of rolls when the magnetic field intensity is increased.

Our purpose in this paper is the better understanding of the action of a constant and uniform magnetic field on convective instabilities in cylindrical cavities heated from below. The pure thermal case without magnetic field has been studied in Part I.[10] In this study, all the boundaries are considered to be electrically insulating and the magnetic Reynolds number is small enough to neglect the perturbations of the applied magnetic field due to the fluid flow. For both orientations of the magnetic field (vertical and horizontal), the results of stabilization are presented through stability diagrams giving the evolution of the primary thresholds as a function of the aspect ratio A and the Hartmann number Ha. Beyond the primary thresholds, the study is focused on the effect of the magnetic field on the secondary bifurcation found in the pure thermal case, for $A=0.5$, and given in the first part of this paper.[10]

II. MATHEMATICAL MODEL

We consider an incompressible fluid confined in a vertical cylindrical cavity of aspect ratio $A=H/D$ where H is the height and D is the diameter (Fig. 1). The two ends of the cylinder are supposed to be isothermal with the lower end held at temperature T_h, which is greater than the temperature T_c of the upper end. The sidewalls are considered to be adiabatic. The fluid is assumed to be Newtonian and electrically conducting. There may be a uniform magnetic field B_0 which generates a damping Lorentz force through the electric currents induced by the motion across the magnetic field. All the physical properties are assumed to be constant, except the density which varies linearly with temperature in the buoyancy term (Boussinesq approximation): $\rho=\rho_0(1-\beta(T-T_0))$, where β is the thermal expansion coefficient and T_0 is the mean temperature: $T_0=(T_h+T_c)/2$.

The governing equations for the temperature T, pressure p, and velocity $\boldsymbol{u}$ are the Navier–Stokes equations coupled with the energy equation. By scaling length with the diameter D of the cylinder, time with D^2/ν, velocity with $U_{\mathrm{ref}}=\nu\cdot \mathrm{Gr}/D$, the magnetic flux density with B_0, electric current density with $\sigma_e U_{\mathrm{ref}}\cdot B_0$, and by introducing the dimensionless temperature field as $\theta=A(T-T_0)/(T_h-T_c)$, the equations, including the Lorentz force, can be written in their dimensionless form as

$$\frac{\partial \boldsymbol{u}}{\partial t}=-\mathrm{Gr}(\boldsymbol{u}\cdot\nabla)\boldsymbol{u}-\nabla p+\nabla^2\boldsymbol{u}+\theta\hat{z}+\mathrm{Ha}^2\boldsymbol{J}\times e_{\boldsymbol{B}0}, \tag{1}$$

$$\nabla\cdot\boldsymbol{u}=0, \tag{2}$$

$$\frac{\partial\theta}{\partial t}=-\mathrm{Gr}\,\boldsymbol{u}\cdot\nabla\theta+\frac{1}{\mathrm{Pr}}\nabla^2\theta, \tag{3}$$

where Gr, Ha, and Pr are the Grashof, Hartmann, and Prandtl numbers defined respectively as $\mathrm{Gr}=g\beta(T_h-T_c)D^4/H\nu^2$, $\mathrm{Ha}=B_0D(\sigma_e/\rho\nu)^{1/2}$, and $\mathrm{Pr}=\nu/\kappa$. We can also define the Rayleigh number as $\mathrm{Ra}=\mathrm{Gr}\,\mathrm{Pr}$. In these relations, κ is the thermal diffusivity, ν the kinematic viscosity, σ_e the electrical conductivity, and $e_{\boldsymbol{B}0}$ the unit vector in the direction of $\boldsymbol{B}_0$.

The magnetic field density vector $\boldsymbol{B}$ is set equal to $\boldsymbol{B}_0$ (the applied magnetic field) since the induced field $\boldsymbol{b}$ is small for $\mathrm{Re}_m\ll 1$, where Re_m is the magnetic Reynolds number. The dimensionless electric current density $\boldsymbol{J}$ is given by Ohm's law for a moving fluid:

$$\boldsymbol{J}=\boldsymbol{E}+\boldsymbol{u}\times\boldsymbol{e}_{\boldsymbol{B}0}, \tag{4}$$

where $\boldsymbol{E}$ is the electric field normalized by $U_{\mathrm{ref}}B_0D$. Since $\mathrm{Re}_m\ll 1$, the unsteady induced field $\boldsymbol{b}$ is negligible and the electric field can be written as the gradient of an electric potential ($\boldsymbol{E}=-\nabla\Phi_e$). The conservation of the electric current density gives

$$\nabla\cdot\boldsymbol{J}=0, \tag{5}$$

which, combined with (4), leads to

$$\nabla^2\Phi_e=\nabla\cdot(\boldsymbol{u}\times\boldsymbol{e}_{\boldsymbol{B}0}). \tag{6}$$

Concerning the boundary conditions, the velocity is zero (no slip boundary condition) along the boundaries ($z=0$, $z=H$, and $r=R$, where $R=D/2$). The temperature is prescribed at the top (T_c) and at the bottom (T_h), whereas the normal heat flux is zero along the lateral wall ($r=R$). For the electric current density $\boldsymbol{J}$, the normal flux is also zero along all the boundaries. Therefore, in their dimensionless form, the boundary conditions can be written as follows:

$$at\ \ r=\frac{1}{2},\quad u=v=w=\boldsymbol{J}_r=0,\quad \frac{\partial\theta}{\partial r}=0, \tag{7}$$

$$at\ \ z=0,\quad u=v=w=\boldsymbol{J}_z=0,\quad \theta=A/2, \tag{8}$$

$$at\ \ z=A,\quad u=v=w=\boldsymbol{J}_z=0,\quad \theta=-A/2. \tag{9}$$

TABLE I. Tests of numerical accuracy for the case with vertical magnetic field. Primary thresholds Ra_c, corresponding to the critical modes ($m=0$ for $A=0.5$ and $m=1$ for $A=1$) for $Ha=25(n_x+1=n_y+1=9)$.

n_z+1	$A=0.5(m=0)$	$A=1(m=1)$
9	79 191	⋯
11	82 601	9464
13	83 153	10 652
15	⋯	10 767

Solving the above system for $\boldsymbol{u}=\mathbf{0}$, we get the temperature profile of the static solution $\theta(z)=(A/2-z)$, which corresponds to the diffusive regime.

III. NUMERICAL METHODS

The numerical methods presented in this section are given with more details in the first part of this paper.[10] To solve the governing equations we use two different methods: the direct numerical simulation with time stepping, and Newton's method. For the time discretization, at each time step, we first treat the nonlinear terms, then the pressure term, and finally the linear terms.[11] For the spatial discretization, a multidomain pseudo-spectral method is applied to approximate the solution $\boldsymbol{U}(\boldsymbol{u},p,T)$ by its value at some Legendre–Gauss–Lobatto collocation points.[12,13] To construct bifurcation diagrams giving the nonlinear evolution of the convection beyond its onset, we use a continuation method combined with Newton's solver.[14] This method is extended to the direct computation of the primary thresholds, as it is done in Ref. 15. To check the stability of the solutions, we need to calculate the most important modes of the full Jacobian of the governing equations; for this we use Arnoldi's method.[16]

To study the effect of the mesh on the numerical accuracy, we present in Table I, for the vertical magnetic field and $Ha=25$, the primary thresholds Ra_c corresponding to the critical modes ($m=0$ for $A=0.5$ and $m=1$ for $A=1$) for different meshes. For $A=0.5$, when the grid is refined from $9\times9\times11$ to $9\times9\times13$ mesh points per element (respectively for the x, y, and z directions), the variation of $Ra_{c(m=0)}$ is about 0.66%. For $A=1$, the increase of the mesh points per element from $9\times9\times13$ to $9\times9\times15$ implies a variation of 1.02% for $Ra_{c(m=1)}$. Therefore, for the results presented in this paper, we use $9\times9\times13$ mesh points per element for $A=0.5$ and $9\times9\times15$ mesh points per element for $A=1$.

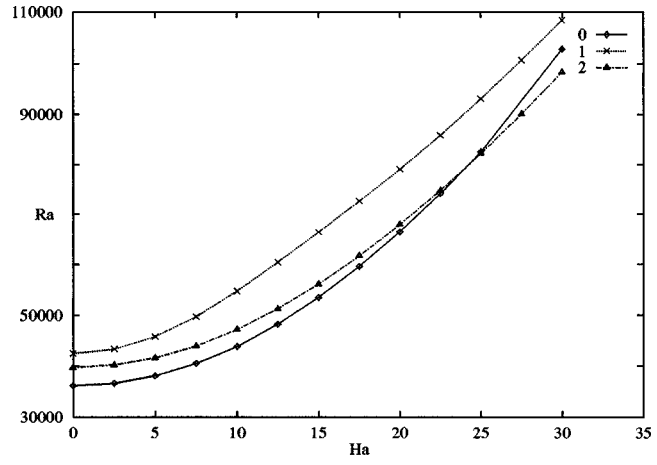

FIG. 2. Effect of the vertical magnetic field on the onset of convection for $A=0.5$. Evolution of the primary thresholds Ra_c, corresponding to the modes $m=0$, $m=1$, and $m=2$, as a function of the Hartmann number, Ha.

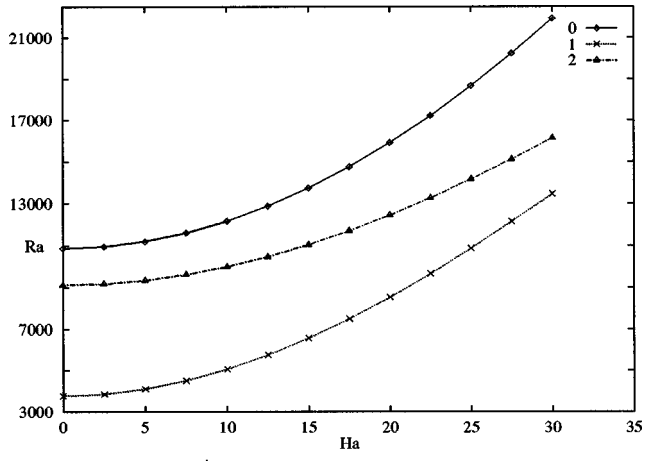

FIG. 3. Effect of the vertical magnetic field on the onset of convection for $A=1$. Evolution of the primary thresholds Ra_c, corresponding to the modes $m=0$, $m=1$, and $m=2$, as a function of the Hartmann number, Ha.

IV. RESULTS

A. Vertical magnetic field

1. Effect on the onset of convection

The use of the vertical magnetic field keeps the same symmetries as in the pure thermal case. So, similarly, two solutions are obtained for the mode $m=0$ (with opposite senses of rotation), and an infinite number of solutions, deduced by azimuthal rotation, for the asymmetric modes $m=1$ and $m=2$. To show the effect of the vertical magnetic field on the onset of convection, we present in Figs. 2 and 3

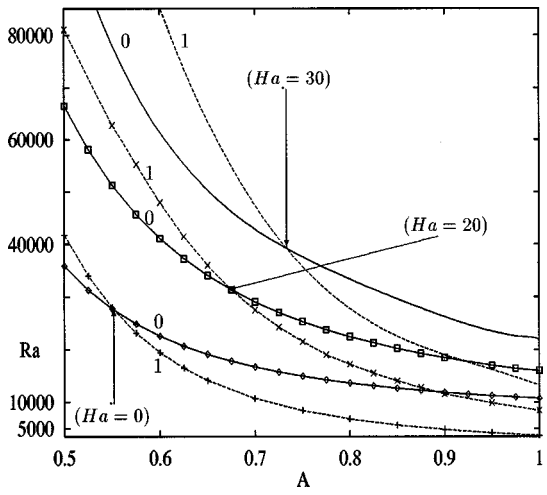

FIG. 4. Influence of the vertical magnetic field on the order of appearance of the modes. Evolution of the primary thresholds Ra_c, corresponding to the modes $m=0$ and $m=1$ for $Ha=0$, 20, and 30, as a function of the aspect ratio, A.

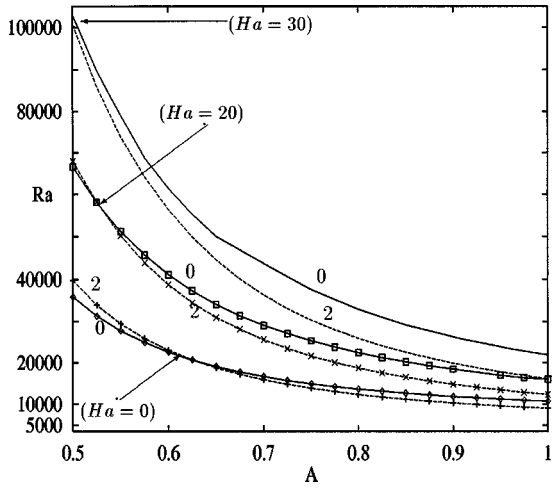

FIG. 5. Influence of the vertical magnetic field on the order of appearance of the modes. Evolution of the primary thresholds Ra_c, corresponding to the modes $m=0$ and $m=2$ for Ha=0, 20, and 30, as a function of the aspect ratio, A.

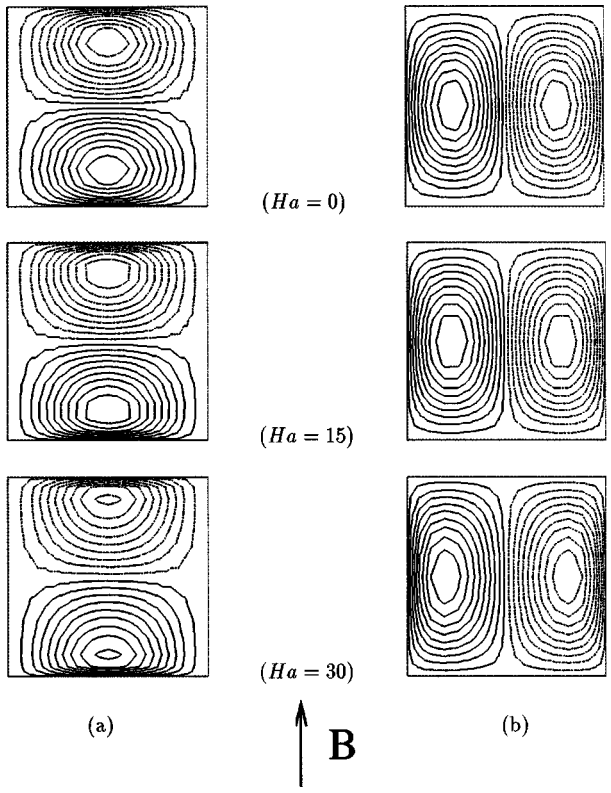

FIG. 6. Effect of the vertical magnetic field on the structure of the flow. (a) Iso-u in the vertical symmetry plane P_{VS} showing the evolution of δ_H. (b) Iso-w in the same plane showing the evolution of $\delta_\parallel$ (critical modes $m=1$ for $A=1$).

the evolution of the primary thresholds as a function of the Hartmann number Ha for respectively $A=0.5$ and $A=1$. These stability curves show that all the modes are stabilized by the vertical magnetic field. However, they are not equally stabilized, the mode $m=2$ being the less stabilized mode. An important consequence is that for $A=0.5$ convection sets in with the mode $m=2$ beyond Ha=24. The evolution of the primary thresholds as a function of the aspect ratio A is given in Figs. 4 and 5, respectively, for the modes $m=0$ and $m=1$ and for the modes $m=0$ and $m=2$. We see that the critical aspect ratio at which the intersection occurs between the modes $m=0$ and $m=1$ increases with Ha (Fig. 4), whereas the critical aspect ratio corresponding to the intersection between the modes $m=0$ and $m=2$ decreases with Ha (Fig. 5). We can therefore conclude that the vertical magnetic field stabilizes the mode $m=0$ less than the mode $m=1$, and more than the mode $m=2$, and that the range of A for which the critical mode is $m=2$ increases with Ha.

To analyze the effect of the vertical magnetic field on the flow, we show in Fig. 6 the isovalues of u (a) and w (b) in the vertical symmetry plane P_{VS}, for the critical mode $m=1$

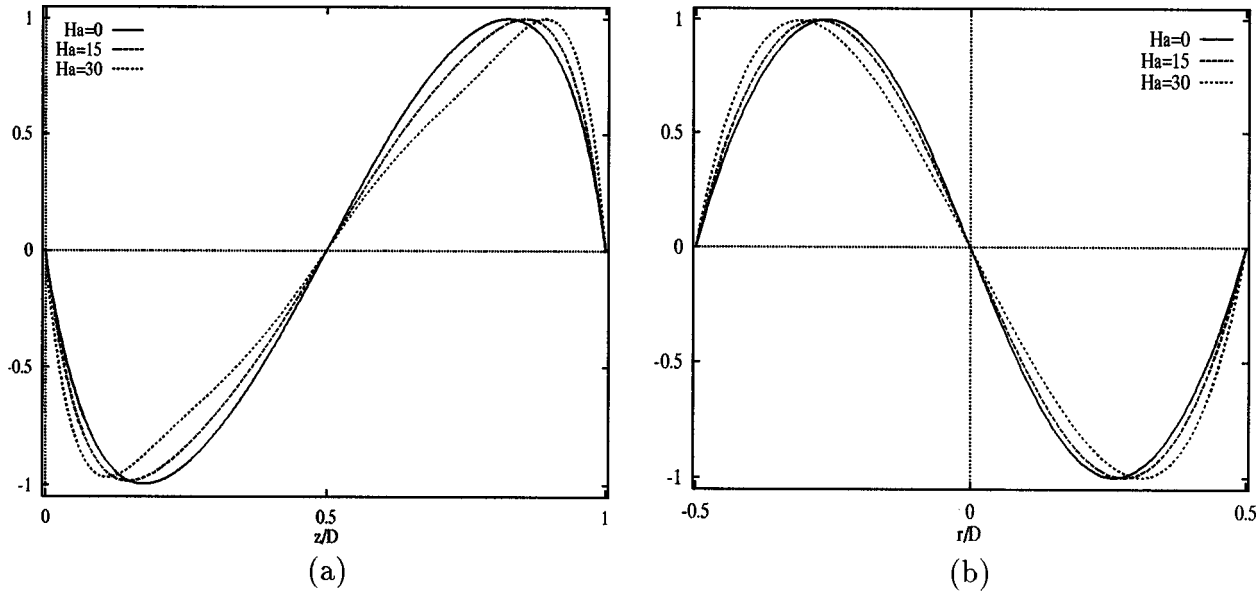

FIG. 7. Effect of the vertical magnetic field on the structure of the flow. (a) Profiles of u on the axis of the cylindrical cavity. (b) Profiles of w on the horizontal axis given by the intersection of the planes P_H and P_{VS} (critical modes $m=1$ for $A=1$).

TABLE II. Values of δ_H and $\delta_\parallel$ for Ha=0, 15, and 30, for the critical mode $m=1$ with vertical magnetic field ($A=1$).

Ha	δ_H	$\delta_\parallel$
0	0.177	0.237
15	0.145	0.207
30	0.107	0.188

($A=1$) at Ha=0, 15, and 30. The evolution of the Hartmann layers (along the horizontal boundaries) can be observed in Fig. 6(a) and the evolution of the parallel layers (along the vertical boundaries) in Fig. 6(b). According to these figures, the thickness of both layers, respectively δ_H and $\delta_\parallel$, decreases when Ha is increased, but the evolution of the Hartmann layer is quicker. A better estimation of the evolution of δ_H and $\delta_\parallel$ can be obtained from Fig. 7 where are given, for Ha=0, 15, and 30, the profiles of u on the axis of the cavity and w on the horizontal axis at the intersection between P_H and P_{VS} planes. The values of δ_H and $\delta_\parallel$, measured on these profiles as the distance between the boundaries and respectively the maximum of u and w, are given in Table II. As expected, the decrease of δ_H for increasing Ha is stronger than that of $\delta_\parallel$. However, these variations are not yet in the asymptotic regime where, according to the literature,[17] δ_H and $\delta_\parallel$ vary as Ha^{-1} and $\mathrm{Ha}^{-1/2}$, respectively.

2. Effect on the secondary bifurcation

For $A=0.5$, we obtain the same secondary bifurcation as in the pure thermal case, namely a transition from the axisymmetric mode $m=0$ to an asymmetric mode $m=02$ triggered by a $m=2$ perturbation. The effect of the vertical magnetic field on this secondary bifurcation is shown in Fig. 8 by the evolution of the secondary threshold $\mathrm{Ra}c_2$ as a function of the Hartmann number Ha, for Pr=1. On the same plot, we also give the evolution of the primary thresholds corresponding to the modes $m=0$ and $m=2$ (denoted $\mathrm{Ra}c_{(m=0)}$ and $\mathrm{Ra}c_{(m=2)}$, respectively). It can observed that the difference $(\mathrm{Ra}c_2-\mathrm{Ra}c_{(m=0)})$ decreases with the increase of Ha, indicating that the vertical magnetic field is unfavorable to the axisymmetric flow. We also notice that the primary bifurcations $\mathrm{Ra}c_{(m=0)}$ and $\mathrm{Ra}c_{(m=2)}$ intersect with the secondary bifurcation $\mathrm{Ra}c_2$ at Ha=24. It is a classical result that secondary bifurcations can appear or disappear at the intersection of primary bifurcations.[18] Beyond this intersection, the emerging flow is expected to be a $m=2$ mode.

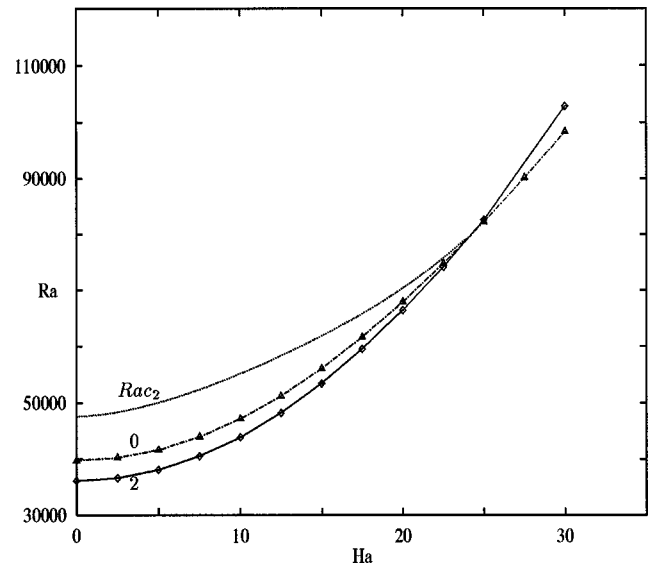

FIG. 8. Effect of the vertical magnetic field on the secondary bifurcation for $A=0.5$ and Pr=1. Evolution of the secondary threshold $\mathrm{Ra}c_2$, and the primary thresholds corresponding to the modes $m=0$ and $m=2$, as a function of the Hartmann number, Ha.

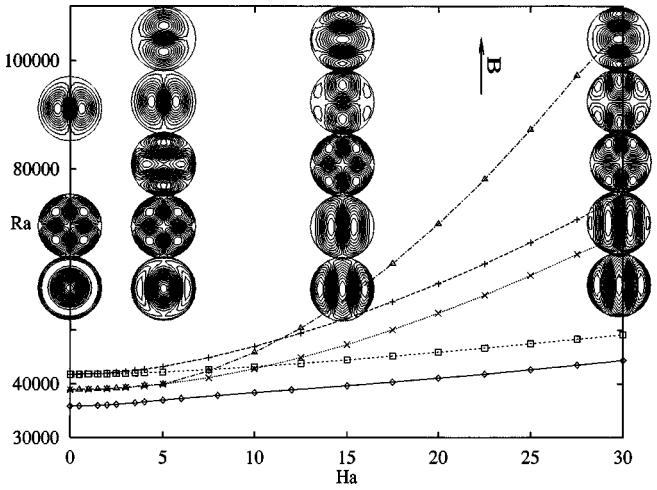

FIG. 9. Effect of the horizontal magnetic field on the onset of convection for $A=0.5$. Evolution of the primary thresholds Ra_c, corresponding to the most important modes, as a function of the Hartmann number, Ha (the plots of iso-w in the plane P_H are given with respect to the order of appearance of the corresponding modes).

B. Horizontal magnetic field

The use of the horizontal magnetic field changes the symmetries of the physical situation. Only three reflections are kept: a reflection with respect to the horizontal midplane P_H (up–down symmetry), and two reflections with respect to

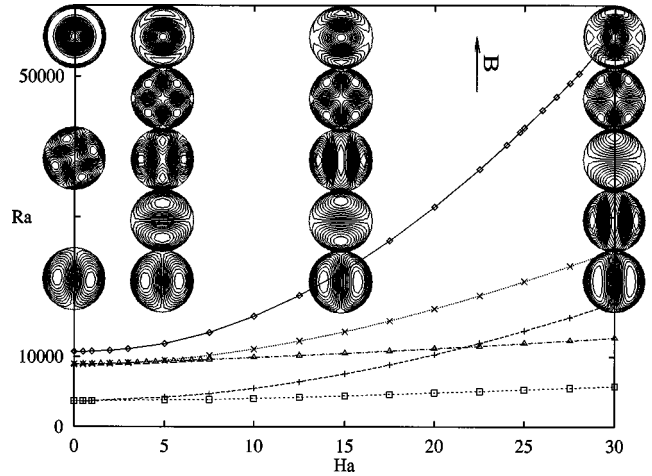

FIG. 10. Effect of the horizontal magnetic field on the onset of convection for $A=1$. Evolution of the primary thresholds Ra_c, corresponding to the most important modes, as a function of the Hartmann number, Ha (the plots of iso-w in the plane P_H are given with respect to the order of appearance of the corresponding modes).

vertical midplanes, the plane parallel to the direction of the magnetic field $P_{\parallel}$, and the plane orthogonal to this direction $P_{\perp}$. The symmetry group of the static solution, which was $\mathcal{O}(2)\times\mathcal{Z}(2)$ in the pure thermal case, is then $\mathcal{Z}(2)\times\mathcal{Z}(2)\times\mathcal{Z}(2)$.[19] Because the onset of convection breaks the up–down symmetry, all the primary bifurcations will be pitchfork bifurcations.

1. Effect on the onset of convection

The effect of the horizontal magnetic field on the onset of convection is given in Figs. 9 and 10, respectively, for $A=0.5$ and $A=1$, by the evolution of the primary thresholds (critical number Ra_c) as a function of the Hartmann number Ha. The corresponding eigenvectors are shown through contour plots of the vertical velocity w in the plane P_H. For $\mathrm{Ha}=0$, the results are those of the pure thermal case: for $A=0.5$, convection sets in with the axisymmetric mode ($m=0$) followed by the modes $m=2$ and $m=1$, and for $A=1$, convection sets in with the mode $m=1$ followed by the modes $m=2$ and $m=0$. All the primary thresholds increase with the Hartmann number, confirming the phenomenon of stabilization of the convection by the application of the magnetic field.

When the horizontal magnetic field is applied the axisymmetric mode disappears because the azimuthal invariance is no longer valid. This mode is transformed into a new oriented mode consisting of two counter-rotating rolls and identified as $m=02$. We notice that, for $A=0.5$, the new mode has the axis of the rolls parallel to $\boldsymbol{B}$, and the mode will be called ''$m=02_{\parallel}$,'' whereas for $A=1$, the axis of the rolls is orthogonal to $\mathbf{B}$ and the mode will be called ''$m=02_{\perp}$.'' Concerning the modes $m=2$ and $m=1$, they were multiply defined for $\mathrm{Ha}=0$. When the horizontal magnetic field is applied, the stabilization of the mode $m=1$ gives two modes, $m=1_{\parallel}$ and $m=1_{\perp}$. For the mode $m=2$, the stabilization also gives two modes: $m=2$ and $m=02_{\perp}$ for $A=0.5$, and $m=02_{\parallel}$ and $m=2$ for $A=1$. All these modes evolve with increasing Ha: the main effects which can be observed in Figs. 9 and 10 are the creation of Hartmann and parallel layers along the lateral boundary, respectively orthogonal and parallel to $\boldsymbol{B}$, and the lengthening in the direction of $\boldsymbol{B}$ of the rolls with axis parallel to $\boldsymbol{B}$.

The intersections between the curves show that the order of appearance of these five modes changes when Ha is increased (the contour plots of the vertical velocity w in the plane P_H, for the corresponding eigenvectors, are given with respect to this order). As a general rule, these modes are strongly stabilized if the axis of the rolls is perpendicular to $\boldsymbol{B}$, and weakly if the axis is parallel to $\boldsymbol{B}$. Thus, convection sets in with the ''parallel'' modes, the mode $m=02_{\parallel}$ for $A=0.5$ and the mode $m=1_{\parallel}$ for $A=1$. These results are coherent with the phenomenon of two-dimensional turbulence observed in turbulent flows under magnetic field.[17]

To study the effect of the horizontal magnetic field on the transition of critical mode when changing the aspect ratio, we give in Fig. 11 the evolution of the primary thresholds corresponding to these critical modes, for $\mathrm{Ha}=0$ and $\mathrm{Ha}=30$, as a function of the aspect ratio A. This figure shows

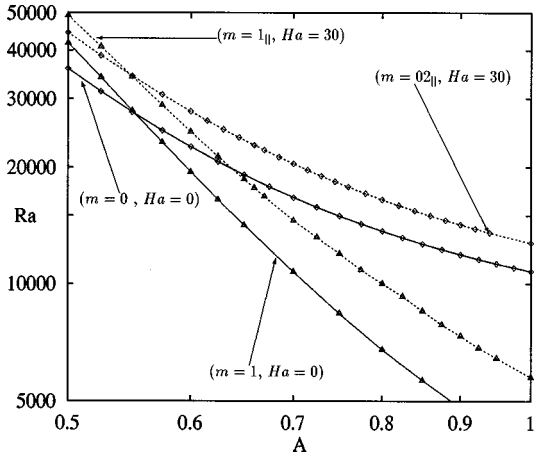

FIG. 11. Influence of the horizontal magnetic field on the transition of the emerging flow structure (given by the critical mode) when varying the aspect ratio, A. Evolution of the primary thresholds Ra_c, corresponding to the modes $m=0$ and $m=1$ for $\mathrm{Ha}=0$, and $m=02_{\parallel}$ and $m=1_{\parallel}$ for $\mathrm{Ha}=30$, as a function of A.

that the transition of critical mode occurs at the same critical value as in the pure thermal case, $A_c=0.55$. This result seems to indicate that both modes, which are ''parallel'' modes, are quite similarly stabilized.

For a better understanding of the change of stabilization of the axisymmetric mode, from $m=02_{\parallel}$ for $A=0.5$ to $m=02_{\perp}$ for $A=1$, we present in Fig. 12 the evolution with A of the primary thresholds corresponding to the modes $m=0$ and $m=2$ for the pure thermal case, and $m=02_{\parallel}$, $m=2$ and $m=02_{\perp}$ for $\mathrm{Ha}=10$. For $\mathrm{Ha}=0$, an intersection occurs between the two curves at $A=0.63$. When the horizontal magnetic field is applied, this intersection disappears. This could be related to the fact that the new solutions $m=02_{\parallel}$ and $m=02_{\perp}$ have the same symmetries.[20] For $A<0.63$, where the mode $m=0$ is more unstable than $m=2$ in the pure thermal case, the stabilization gives $m=02_{\parallel}$ (the less stabilized mode) for the mode $m=0$, and $m=2$ and $m=02_{\perp}$ for the mode $m=2$. On the contrary, for $A>0.63$ the stabilization gives $m=02_{\perp}$ (the most stabilized mode) for the mode m

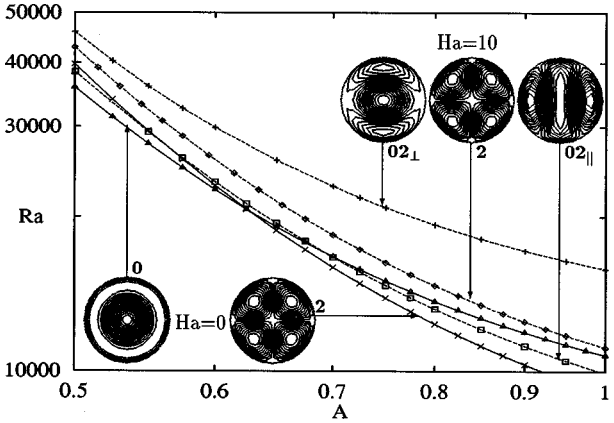

FIG. 12. Stabilization of the modes $m=0$ and $m=2$ by the horizontal magnetic field. Evolution of the primary thresholds Ra_c, corresponding to the modes $m=0$ and $m=2$ for $\mathrm{Ha}=0$, and the modes $m=02_{\parallel}$, $m=2$, and $m=02_{\perp}$ for $\mathrm{Ha}=10$, as a function of the aspect ratio, A.

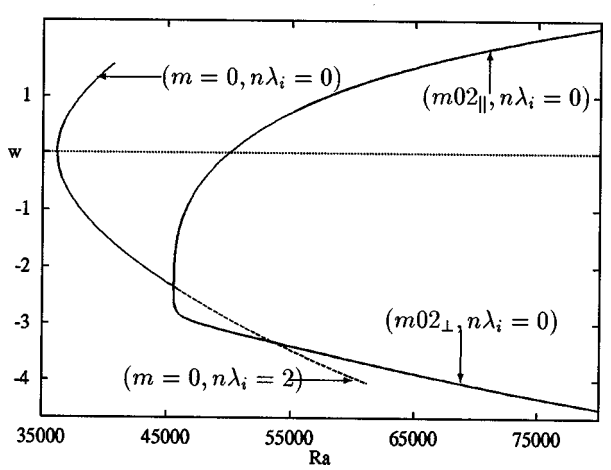

FIG. 13. Bifurcation diagram for the pure thermal case (Ha=0). Evolution of the vertical velocity w at a fixed point as a function of Ra, for $A=0.5$ and Pr=1 ($n\lambda_i$=number of unstable eigenvalues).

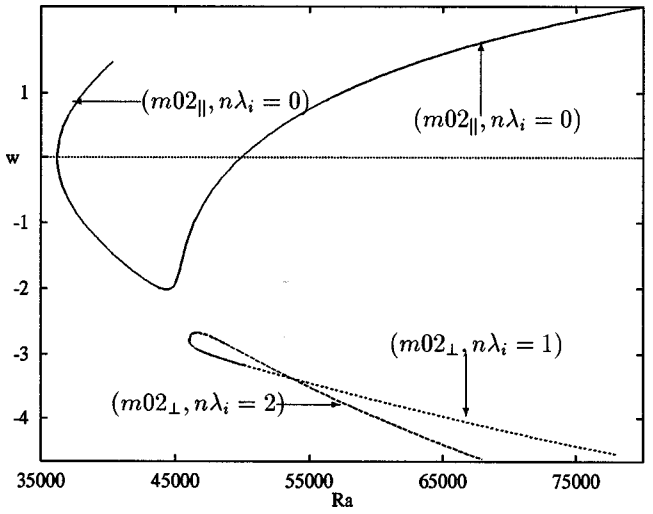

FIG. 14. Bifurcation diagram with horizontal magnetic field (Ha=1). Evolution of the vertical velocity w at a fixed point as a function of Ra, for $A=0.5$ and Pr=1 ($n\lambda_i$=number of unstable eigenvalues).

$=0$, and $m=02_{\parallel}$ and $m=2$ for the mode $m=2$. It is then found that the modes $m=0$ and $m=2$ have to be considered as a whole, and that under horizontal magnetic field they give three modes ($m=02_{\parallel}$, $m=2$, and $m=02_{\perp}$,) the less stabilized being always the ''parallel'' mode ($m=02_{\parallel}$) and the most stabilized the ''orthogonal'' mode ($m=02_{\perp}$).

2. Effect on the secondary bifurcation

For $A=0.5$, without magnetic field, the axisymmetric mode loses its stability at a secondary bifurcation and the new three-dimensional stable solution is identified as an $m=02$ mode. Because of the invariance with azimuthal rotation of our situation, beyond $\mathrm{Ra}c_2$, the critical Rayleigh number corresponding to this transition, an infinite number of such solutions are obtained (circular pitchfork bifurcation). Nevertheless, to make the comparison with the case of the horizontal magnetic field easier, we present in Fig. 13 this secondary bifurcation, for Ha=0 and Pr=1, with only two branches of solutions corresponding to the modes $m=02_{\parallel}$ and $m=02_{\perp}$.

When the horizontal magnetic field is applied, the structure of the emerging flow (from diffusive state) corresponds to the mode $m=02_{\parallel}$. In terms of symmetries, the magnetic field breaks the symmetries broken by the secondary bifurcation in the pure thermal case. Thus, the secondary bifurcation disappears, and, as shown in Fig. 14, two disconnected branches are obtained, the signature of an imperfect bifurcation. The first branch, which is stable, is the continuation of the emerging flow and corresponds then to the mode $m=02_{\parallel}$. The second branch, which appears at a saddle point characterized by a critical Rayleigh number $\mathrm{Ra}c_2'$ and which corresponds to the mode $m=02_{\perp}$, can be considered as the connection of two parts. The first part [$m=02_{\perp}(1)$] results from the stabilization of the unstable axisymmetric solution and is two time unstable. The second part [$m=02_{\perp}(2)$] results from the stabilization of the stable $m=02_{\perp}$ branch and is one time unstable. In Fig. 15, we give the evolution of the imperfect bifurcation for increasing Ha (Ha=0.5, 1, 2, and 3). The projection used in these bifurcation diagrams is different from that used in Figs. 13 and 14. This figure shows that $\mathrm{Ra}c_2'$ increases with Ha, and that the original shape of the perfect bifurcation is quite quickly lost.

3. Theoretical analysis

The aim of this section is to present a theoretical model which can explain the imperfect bifurcation obtained with the horizontal magnetic field. The perfect symmetry-breaking bifurcation obtained in the pure thermal case corresponds to a circular pitchfork bifurcation (which will be first detailed), and the imperfection (due to the horizontal magnetic field) is introduced as a small constant parameter ϵ. The model is then given by the following algebraic equation:

$$\frac{dS}{dt}=\mu S-|S|^2S+\epsilon, \tag{10}$$

where S, the solution, is assumed to be complex and μ is the continuation parameter. Replacing S by $\mathrm{Re}^{i\phi}$ in Eq. (10) leads to

$$\begin{aligned}\frac{dR}{dt}&=\mu R-R^3+\epsilon\cos\Phi,\\ \frac{d\Phi}{dt}&=-\epsilon\frac{\sin\Phi}{R}.\end{aligned} \tag{11}$$

The steady solutions of this system are given by

$$\begin{aligned}&\Phi_0=0, \quad \mu R-R^3+\epsilon=0,\\ &\Phi_0=\pi, \quad \mu R-R^3-\epsilon=0.\end{aligned} \tag{12}$$

a) Circular-pitchfork bifurcation (pure thermal case). For $\epsilon=0$, the solutions are independent of Φ and given by

$$\mu R-R^3=0. \tag{13}$$

They correspond to the trivial solution ($R=0$) and to circles of equivalent solutions ($R=\sqrt{\mu}$). The diagram in Fig. 16(a) gives the evolution of R versus μ for $\epsilon=0$ (view in the cross section at $\Phi=0$ or $\Phi=\pi$). This diagram shows that the

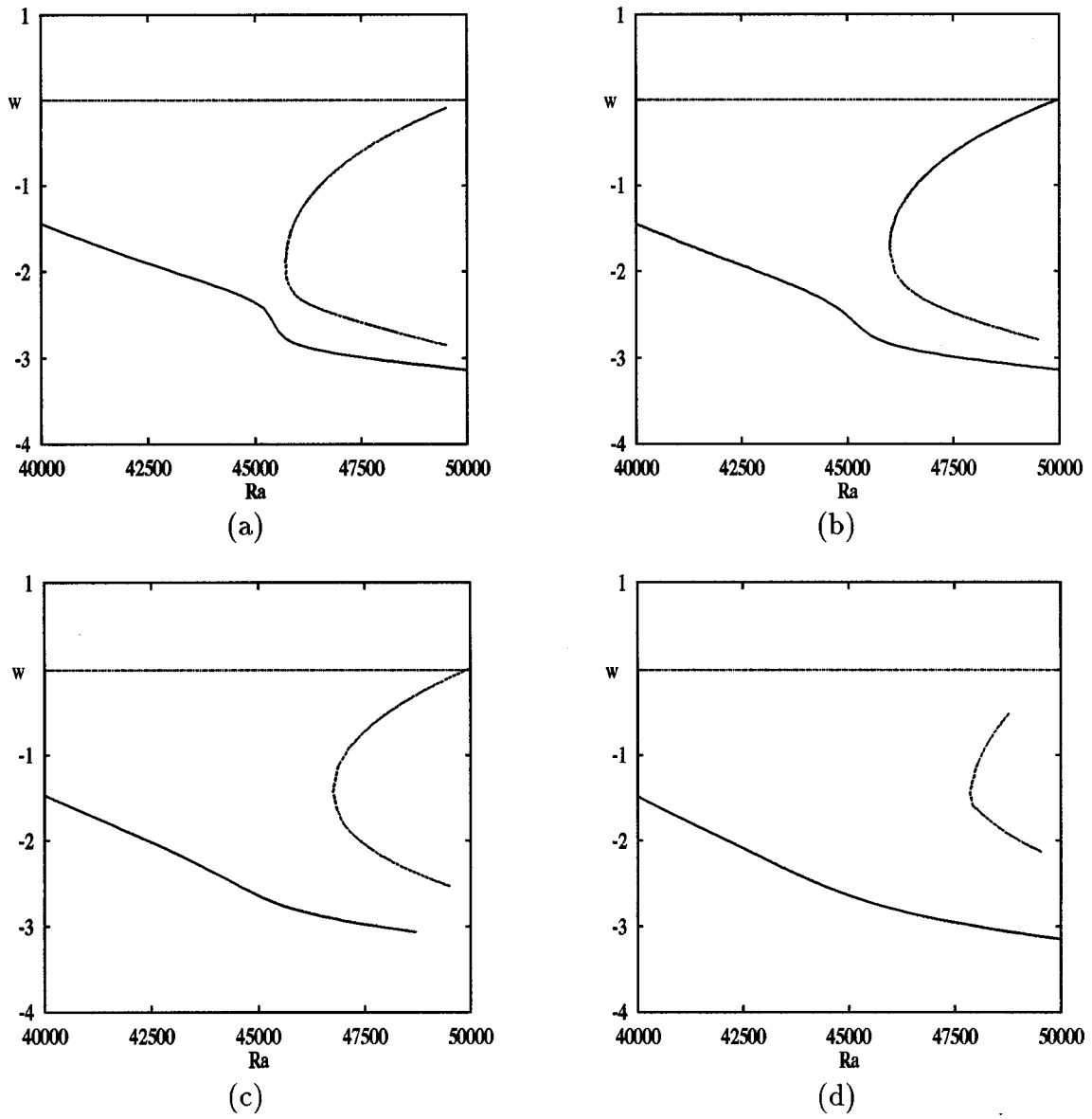

FIG. 15. Effect of the Hartmann number Ha on the imperfect secondary bifurcation for $A=0.5$ and $\mathrm{Pr}=1$. Evolution of the vertical velocity w at a fixed point as a function of Ra. (a) $\mathrm{Ha}=0.5$, (b) $\mathrm{Ha}=1$, (c) $\mathrm{Ha}=2$, and (d) $\mathrm{Ha}=3$. (Note that this figure presents w at a different point in the flow from that used in Fig. 14 and the scale for Ra is different.)

nontrivial solutions are obtained above the critical value $\mu=0$. The phase diagram, presented in Fig. 16(b), shows the circle of stable solutions (attractors) for $\mu=5$. These solutions correspond to the solutions $m=02$ of the pure thermal case. The trivial solution at the center of the circle, which corresponds to the solution $m=0$ of the pure thermal case, is repulsive in two perpendicular directions, and thus is two time unstable. The attraction to the circle of stable solutions occurs in the radial direction and is independent of the azimuthal direction Φ which is a neutral direction [$d\Phi/dt=0$ obtained from (11)].

b) Imperfect bifurcation (case with horizontal magnetic field). The bifurcation diagram given in Fig. 17(a) is obtained for $\epsilon=3$. The imperfection introduced in the system has the effect of suppressing the invariance with Φ and creating a disconnected branch of solutions. This disconnected branch will exist above a critical value μ_c which depends on $\epsilon(\mu_c=\epsilon^{2/3})$. The characteristics of the three solutions obtained for $\mu>\mu_c$ can be described from the phase diagram given, for $\mu=5$, in Fig. 17(b). On this diagram, the circle represents the points with $dR/dt=0$. The first solution at the top of the circle ($\Phi=0$) is part of the main stable branch which evolves smoothly, and corresponds to the mode $m=02_{\parallel}$ in our problem. This solution is attractive in both R and Φ directions. The second solution inside the circle ($\Phi=\pi$, small R) comes from the trivial state of the perfect case and corresponds to the solution $m=02_{\perp}(1)$ in our problem. This solution is repulsive in the R and Φ directions, and is thus two time unstable. The third solution at the bottom of the circle ($\Phi=\pi$) corresponds to the solution $m=02_{\perp}(2)$ in our problem. This solution is also unstable as it is still attractive in the R direction, but repulsive in the Φ direction. We can see on the phase diagram that there is a global phase shift along the circle from the unstable solution at the bottom of

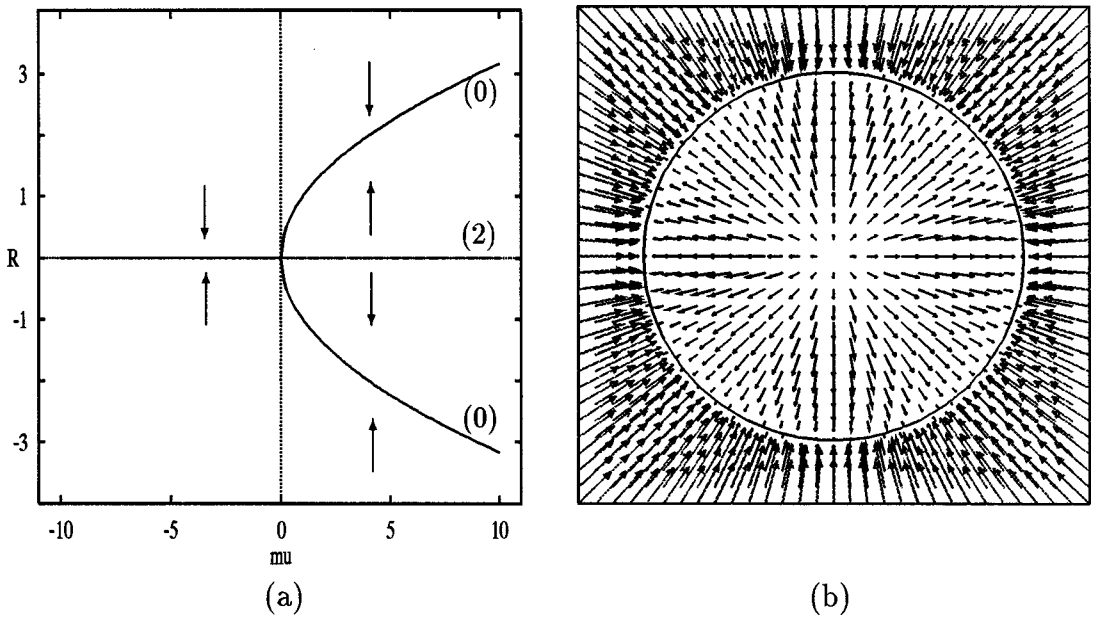

FIG. 16. Theoretical model for the circular-pitchfork-bifurcation. (a) Bifurcation diagram giving the evolution of R versus μ, for $\epsilon=0$. (b) Phase diagram for $\mu=5$.

the circle to the stable solution at the top. This will correspond in our problem to a shift in the azimuthal direction which will globally rotate the $m=02$ modes towards the only stable solution, the $m=02_{\parallel}$ mode. The phase shift along the circle is slow compared to the attraction along the radial direction. This gives for the two (stable and unstable) solutions on the circle, small (respectively negative and positive) eigenvalues connected to the phase shift, and larger (negative) eigenvalues connected to the radial attraction. We have checked that this observation also applies to the two solutions $m=02_{\parallel}$ and $m=02_{\perp}(2)$ of our problem.

C. Analysis of the induced current

For a better understanding of the influence of the magnetic field on the flow, we analyze the induced current which can be written as

$$\boldsymbol{J}=\sigma_e(\boldsymbol{u}\times\boldsymbol{B}-\nabla\Phi_e). \tag{14}$$

The first contribution, $\boldsymbol{J}_1=\sigma_e(\boldsymbol{u}\times\boldsymbol{B})$, called the direct induced current, results from the interaction between the flow of the electro-conducting fluid and the magnetic field $\boldsymbol{B}$. The second contribution, $\boldsymbol{J}_2=-\sigma_e\nabla\Phi_e$, results from the electric

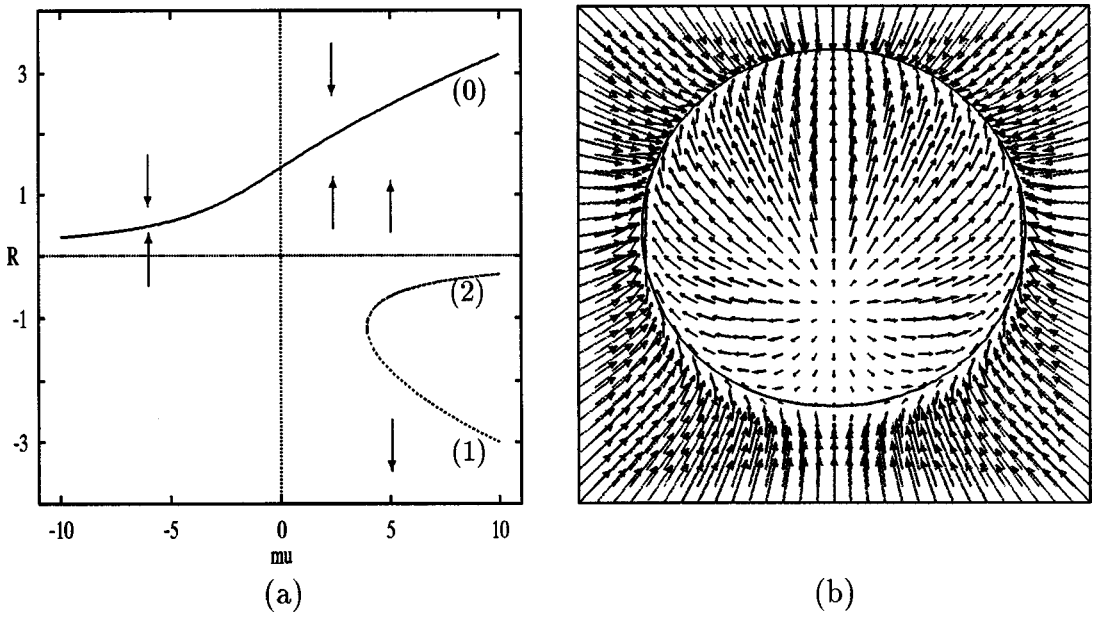

FIG. 17. Theoretical model for the imperfect bifurcation. (a) Bifurcation diagram giving the evolution of R versus μ, for $\epsilon=3$. (b) Phase diagram for $\mu=5$.

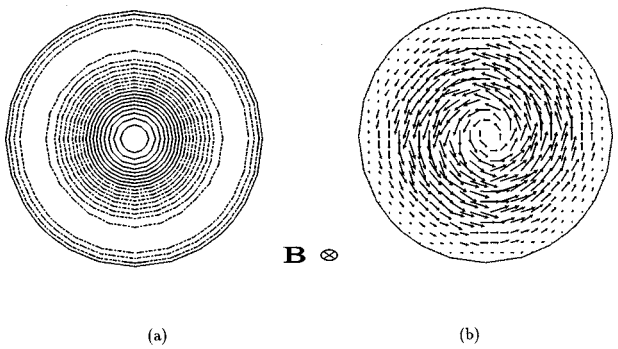

FIG. 18. Analysis of the induced current for the vertical magnetic field. Iso-w (a), and induced electric current $\boldsymbol{J}$ (b) in the plane P_H, for the critical mode $m=0$ ($A=0.5$ and $\mathrm{Ha}=10$).

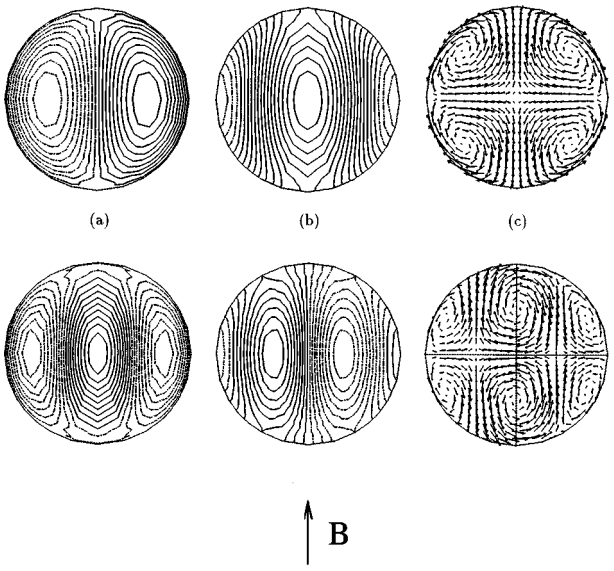

FIG. 19. Analysis of the induced current for the horizontal magnetic field. Iso-w (a), iso- Φ_e (b), and induced electric current $\boldsymbol{J}$ (c) in the plane P_H, for the critical modes at $\mathrm{Ha}=10$: $m=1_{\parallel}$ for $A=1$ (top) and $m=02_{\parallel}$ for $A=0.5$ (bottom).

potential field Φ_e. Some general rules can be first given: $\boldsymbol{J}_1$ is first created by the motion of the fluid. If $\boldsymbol{J}_1$ is not conserved [$\mathrm{div}(\boldsymbol{J}_1)\neq 0$], electric charges driven by $\boldsymbol{J}_1$ accumulate in some parts of the flow creating a global electric potential field Φ_e. This electric potential generates $\boldsymbol{J}_2$ which then allows the global electric current $\boldsymbol{J}$ to be conserved. $\boldsymbol{J}_2$ generally opposes $\boldsymbol{J}_1$ in the zones where $\boldsymbol{J}_1$ is strong, thus diminishing the braking effect. But in the zones where $\boldsymbol{J}_1$ is small, as it insures the conservation of the current, $\boldsymbol{J}_2$ will also very often create current loops, particularly for electrically insulating walls where the conservation of the current has to occur inside the fluid. For such electrically insulating walls, the electric potential Φ_e is then expected to play a greater role than for electrically conducting walls where the current can flow inside the walls, and so the braking of the flow should be weaker.

To illustrate the roles assumed by these two contributions, we show some examples of current circulation for critical modes obtained with vertical or horizontal magnetic field in Figs. 18 and 19.

We first present the axisymmetric mode ($m=0$) for $A=0.5$ with vertical magnetic field ($\mathrm{Ha}=10$) (Fig. 18). Using the axisymmetry of the flow, we can express $\boldsymbol{J}_1$ as

$$\boldsymbol{J}_1=\sigma_e(u_r\mathbf{e_r}+u_z\mathbf{e_z})\times B\mathbf{e_z}=-\sigma_e u_r B\mathbf{e}_\phi, \tag{15}$$

which gives

$$\mathrm{div}\,(\boldsymbol{J}_1)=-\sigma_e\frac{B}{r}\frac{\partial u_r}{\partial\phi}=0. \tag{16}$$

Thus, for this case, the conservation of the induced current occurs naturally without need for $\boldsymbol{J}_2$ and the electric potential Φ_e has no effect on the flow. The induced current corresponding then to $\boldsymbol{J}_1$ is purely azimuthal [Fig. 18(b)].

In Fig. 19 we now present two cases with horizontal magnetic field corresponding to the critical modes $m=1_{\parallel}$ for $A=1$ and $m=02_{\parallel}$ for $A=0.5$. For the mode $m=1_{\parallel}$, Fig. 19(a) shows that the flow goes up in the right-half part and down in the left-half part. This implies that in the P_H plane, $\boldsymbol{J}_1$ is along the x direction, flowing from the lateral boundaries towards the center, which creates a positive electric potential difference between the center and the boundaries [Fig. 19(b)]. $\boldsymbol{J}_2$ is a consequence of this electric potential, opposing $\boldsymbol{J}_1$ in the zones where $\boldsymbol{J}_1$ was strong (middle part of the cavity along the x direction), and driving the current within four loops which insure the global conservation of the current [Fig. 19(c)]. Components of current parallel to $\boldsymbol{B}$ are then created in the middle part of the cavity along the y direction, on which the magnetic field $\boldsymbol{B}$ will have no effect. The mode $m=02_{\parallel}$ presented in Fig. 19 can be considered as the juxtaposition of two counter-rotating rolls quite similar to the $m=1_{\parallel}$ roll. The main electric properties can then be deduced from the previous case. The electric potential has two maxima, each of them centered on the axis of one of the rolls [see the view in the P_H plane in Fig. 19(b)], and the global electric current in the P_H plane presents six loops of current [Fig. 19(c)], which corresponds to the juxtaposition of two times the four loops of the $m=1_{\parallel}$ mode, the co-rotating central loops having merged.

Concerning the symmetry properties of the induced electric current $\boldsymbol{J}$, they are imposed by $\boldsymbol{J}_1$ (as $\boldsymbol{J}_2$ adapts to $\boldsymbol{J}_1$), and can then be easily deduced from the symmetries of the velocity field $\boldsymbol{u}$. It is found that the symmetry properties of $\boldsymbol{u}$ with respect to planes parallel to $\boldsymbol{B}$ are changed for $\boldsymbol{J}$ (symmetry of $\boldsymbol{u}$ gives antisymmetry for $\boldsymbol{J}$, and vice versa), whereas the symmetry properties with respect to planes orthogonal to $\boldsymbol{B}$ are preserved.[21] These properties can be checked by comparing Figs. 18(a) and 18(b) and Figs. 19(a) and 19(c).

D. Energetic analysis

We want to analyze the stabilization of the flow under magnetic field by energetic considerations. We first derive some relations concerning the electric energy. The induced electric current can be expressed as

$$\frac{\boldsymbol{J}}{\sigma_e}=\boldsymbol{E}+\boldsymbol{u}\times\boldsymbol{B}. \tag{17}$$

If we multiply this relation by $\boldsymbol{J}$ and integrate over the liquid volume Ω, we obtain

$$\int_\Omega \boldsymbol{J}\cdot\boldsymbol{E}\, d\Omega = \int_\Omega \frac{\boldsymbol{J}^2}{\sigma_e}\, d\Omega + \int_\Omega \boldsymbol{u}\cdot(\boldsymbol{J}\times\boldsymbol{B})\, d\Omega, \tag{18}$$

which can be written as

$$\mathcal{P}_e = \mathcal{P}_j + \mathcal{P}_m. \tag{19}$$

This relation means that the electric power in the system $\mathcal{P}_e$ is the sum of the power dissipated by the Joule effect $\mathcal{P}_j$ and the power developed by the Lorentz force $\mathcal{P}_m$. Replacing $\boldsymbol{E}$ by $-\nabla\Phi_e$, we can express $\mathcal{P}_e$ as

$$\mathcal{P}_e = -\int_\Omega \boldsymbol{J}\cdot\nabla\Phi_e\, d\Omega$$

$$= -\int_\Omega \nabla\cdot(\Phi_e\boldsymbol{J})\, d\Omega + \int_\Omega \Phi_e(\nabla\cdot\boldsymbol{J})\, d\Omega. \tag{20}$$

These two terms are equal to zero, the first term because all the boundaries are electrically insulating, and the second term because of the continuity equation for the electric current. Thus, the electric power in the system $\mathcal{P}_e$ is equal to zero, and as $\mathcal{P}_j$ is positive, $\mathcal{P}_m$ will be negative [see Eq. (19)]. Energetically, the stabilization of the flow by the magnetic field can be explained by the fact that the power developed by the Lorentz force is added to the viscous dissipation to counterbalance the buoyancy term. To make this point clearer, we will do the same energetic analysis at the primary thresholds as in the pure thermal case.[10] The equation of kinetic energy can be written as

$$I_v + I_b + I_d + I_m = I_k. \tag{21}$$

Here, I_v, I_b, I_d, and I_k (respectively production by the base flow, production by buoyancy, dissipation, and rate of change of kinetic energy) have the same meaning as in the pure thermal case,[10] and I_m is an additional term due to the Lorentz force and defined as

$$I_m = -\mathrm{Ha}^2 \int_\Omega \frac{\boldsymbol{J}^2}{\sigma_e}\, d\Omega. \tag{22}$$

At the steady primary thresholds, $I_v = 0$ (static base state) and $I_k = 0$. By changing the velocity scale to κ/D, this equation can be written as

$$\mathrm{Ra}_c I_b' + I_d' + I_m' = 0 \tag{23}$$

or

$$\mathrm{Ra}_c = \frac{-I_d'}{I_b'} + \frac{-I_m'}{I_b'}. \tag{24}$$

This relation means that the critical Rayleigh is the sum of two positive terms, the first term due to the viscous dissipation, $\mathrm{Ra}c_d$, and the second term due to the power of the Lorentz force, $\mathrm{Ra}c_m$. It is found that when a magnetic field is applied, the $\mathrm{Ra}c_d$ contribution can be changed (positively or negatively) due to the evolution of the flow structure, but the main effect comes from the new Lorentz contribution, $\mathrm{Ra}c_m$, which increases quickly with Ha. In Fig. 20, we present the evolution of $\mathrm{Ra}c_m/\mathrm{Ra}_c$ (in %) versus Ha, for the horizontal magnetic field and the modes $m = 02_\parallel$, $m = 02_\perp$, and $m = 2$. Comparing the contribution of $\mathrm{Ra}c_m$ for these three modes, it is found that this term is the most important for the strongly stabilized mode $m = 02_\perp$ and less important for the weakly stabilized mode $m = 02_\parallel$. The energetic analysis of the stabilization of the modes $m = 0$ and $m = 2$ for a vertical magnetic field ($A = 0.5$) shows a different behavior. In this case, the Lorentz contribution is strong for both modes, but larger for $m = 2$ compared to $m = 0$, which would indicate a larger stabilization of this mode. In fact, the global stabilization effect is stronger for the mode $m = 0$, which allows the mode $m = 2$ to become the critical mode beyond Ha = 24 (Fig. 2). This is due to the variations of the viscous contribution, $\mathrm{Ra}c_d$: these variations are slightly positive for the mode $m = 0$, giving a slight additional stabilization effect, but they are strongly negative for the mode $m = 2$ and contribute to a decrease of the global stabilization effect.

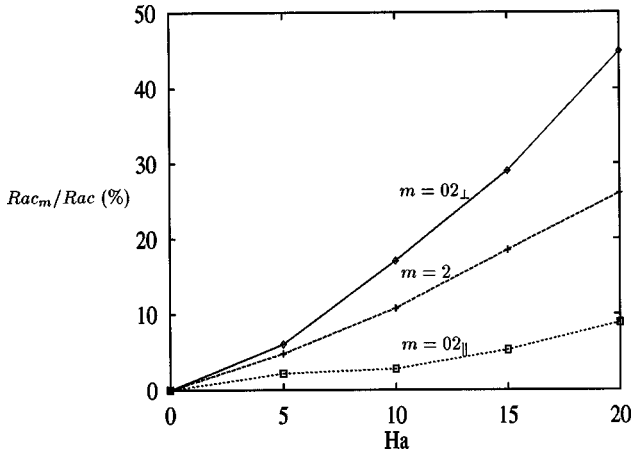

FIG. 20. Evolution of the contribution $\mathrm{Ra}c_m/\mathrm{Ra}_c$ (in %) versus Ha, for the horizontal magnetic field and the three modes $m = 02_\perp$, $m = 2$, and $m = 02_\parallel$.

V. CONCLUSIONS

In this paper, we investigated the effects of a constant and uniform magnetic field on the convection in a cylindrical cavity heated from below. A vertical magnetic field does not change the symmetries which occur in the pure thermal case. Similar convective modes are then obtained, but they are not equally stabilized, so that the mode $m = 2$ becomes a critical mode in the intermediate range of aspect ratio (around $A = 0.55$) for sufficiently large Hartmann number Ha. For $A = 0.5$, the same secondary bifurcation as in the pure thermal case occurs (from $m = 0$ to $m = 02$), but the corresponding threshold increases with Ha.

The use of a horizontal magnetic field reduces the number of symmetries of the system. The axisymmetric mode disappears, giving an asymmetric mode $m = 02$ whereas the other modes ($m = 2$ and $m = 1$) which were multiply defined (to within a rotation) have now two possible orientations well defined with respect to the applied magnetic field **B**. The three original modes ($m = 0$, $m = 1$, and $m = 2$) give then five modes: two $m = 1$ modes ($m = 1_\parallel$ and $m = 1_\perp$), two $m = 02$ modes ($m = 02_\parallel$ and $m = 02_\perp$), and one $m = 2$ mode. These modes are differently stabilized, weakly if the axis of

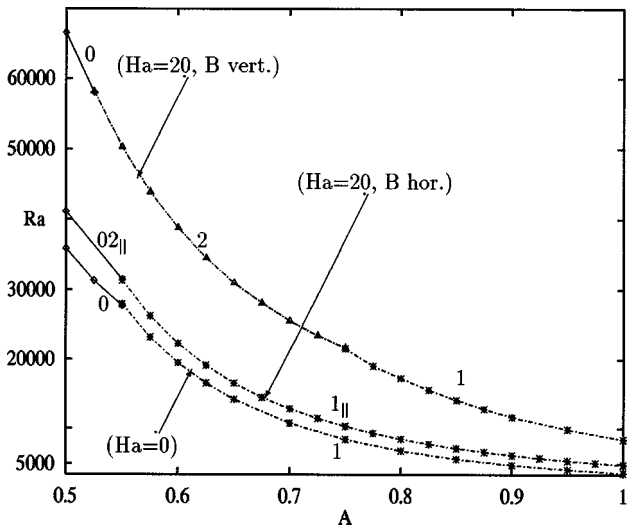

FIG. 21. Comparison of the stabilization by horizontal and vertical magnetic field. Evolution of the critical primary thresholds as a function of the aspect ratio A, at $\mathrm{Ha}=0$ and $\mathrm{Ha}=20$ for both magnetic field orientations.

the rolls is parallel to $\boldsymbol{B}$ and strongly if the axis is perpendicular. For $A=0.5$, convection sets in with a $m=02_{\|}$ mode. The secondary bifurcation then disappears and is replaced by an imperfect bifurcation which we have characterized and modeled.

At last, the effect of stabilization by magnetic field has been interpreted in terms of induced electric current and by energetic considerations.

We conclude this article by a comparison between the stabilizations obtained by vertical and horizontal magnetic fields. As can be seen in Fig. 21 where the critical thresholds are given as a function of the aspect ratio at $\mathrm{Ha}=0$ and $\mathrm{Ha}=20$ for both magnetic field orientations, the stabilization is much stronger with a vertical magnetic field. This fact can be connected to the symmetry properties mentioned in the previous sections. The vertical magnetic field can efficiently act on the different modes because the roll axes are perpendicular to the applied field for every mode. For the horizontal magnetic field, only two orientations of the modes are kept. In fact, one of these situations, which corresponds to rolls with axes parallel to the applied field and will appear as the critical state, is weakly stabilized, leading then to a poor stabilization by horizontal magnetic field.

ACKNOWLEDGMENTS

We wish to thank Professor R. Moreau from MADYLAM, Dr. L. Tuckerman from LIMSI, and Dr. T. Alboussière from Cambridge University for helpful discussions of our results. This work was supported by the ''Centre National des Etudes Spatiales.'' Computations were carried out on a Cray YMP C98 computer, with the support from the CNRS through the IDRIS institute.

[1] H. BenHadid, D. Henry, and S. Kaddeche, ''Numerical study of convection in the horizontal Bridgman configuration under the action of a constant magnetic field. Part 1. Two-dimensional flow,'' J. Fluid Mech. **333**, 23 (1997).

[2] H. BenHadid and D. Henry, ''Numerical study of convection in the horizontal Bridgman configuration under the action of a constant magnetic field. Part 2: Three-dimensional flow,'' J. Fluid Mech. **333**, 57 (1997).

[3] H. BenHadid and D. Henry, ''Numerical simulation of convective three-dimensional flows in a horizontal cylinder under the action of a constant magnetic field,'' J. Cryst. Growth **166**, 436 (1996).

[4] T. Alboussière, J. P. Garandet, and R. Moreau, ''Buoyancy-driven convection with a uniform magnetic field. Part 1. Asymptotic analysis,'' J. Fluid Mech. **253**, 545 (1993).

[5] T. Alboussière, J. P. Garandet and R. Moreau, ''Asymptotic analysis and symmetry in MHD convection,'' Phys. Fluids **8**, 2215 (1996).

[6] V. Bojarevics, ''Horizontal temperature gradient driven flow and its stability in a horizontal channel of rectangular cross-section with the effects of transversal magnetic field,'' in *Advances in Engineering Heat Transfer*, Proceedings Second Baltic Heat Transfer Conference (edited by B. Sunden, E. Blums, and A. Zukauskas) (Computational Mechanics, Southampton, 1995).

[7] S. Chandrasekhar, *Hydrodynamic and Hydromagnetic Stability* (Clarendon, Oxford, 1961).

[8] J. Baumgartl and G. Müller, ''Calculation of the effects of magnetic field damping on fluid flow. Comparison of magnetohydrodynamic models of different complexity,'' In Proceedings 8^{th} European Symposium on Materials and Fluid Sciences in Microgravity (ESA SP-333), p. 161. ESA Publ. Division c/o ESTEC, Noordwijk, The Netherlands (1992).

[9] R. Mössner, Ph.D. Thesis, Karlsruhe Research Center, Germany, 1996.

[10] R. Touihri, H. BenHadid, and D. Henry, ''On the onset of convective instabilities in cylindrical cavities heated from below. I. Pure thermal case,'' Phys. Fluids **11**, 2078 (1999).

[11] G. E. Karniadakis, M. Israeli, and S. A. Orszag, ''High-order splitting method for the incompressible Navier-Stokes equations,'' J. Comput. Phys. **97**, 414 (1991).

[12] A. T. Patera, ''A spectral element method for fluid dynamics: laminar flow in channel expansion,'' J. Comput. Phys. **54**, 468 (1984).

[13] K. Z. Korczak and A. T. Patera, ''An isoparametric spectral element method for solution of the Navier-Stokes equations in complex geometry,'' J. Comput. Phys. **62**, 361 (1986).

[14] H. B. Keller, ''Numerical solution of bifurcation and nonlinear eigenvalue problems,'' in *Application of Bifurcation Theory*, edited by P. Rabinowitz (Academic, New York, 1977).

[15] A. Bergeon, D. Henry, H. BenHadid, and L. S. Tuckerman, ''Marangoni convection in binary mixtures with Soret effect,'' J. Fluid Mech. **375**, 143 (1998).

[16] N. Nayar and J. M. Ortega, ''Computation of selected eigenvalues of generalized eigenvalue problems,'' J. Comput. Phys. **108**, 8 (1993).

[17] R. Moreau, *Magnetohydrodynamics* (Kluwer Academic, London, 1990).

[18] H. A. Dijkstra, ''On the structure of cellular solutions in Rayleigh-Bénard-Marangoni flows in small aspect ratio containers,'' J. Fluid Mech. **243**, 73 (1992).

[19] M. Golubitsky, I. Stewart, and D. Schaeffer, *Singularities and groups in bifurcation theory, Vol. II* (Springer Verlag, New York, 1988).

[20] K. A. Cliffe and K. H. Winters, ''The use of symmetry in bifurcation calculations and its application to the Bénard problem,'' J. Comput. Phys. **67**, 310 (1986).

[21] R. Touihri, ''Analyse de stabilité des écoulements dans une cavité cylindrique chauffée par le bas en présence d'un champ magnétique,'' Ph.D. Thesis, Ecole Centrale de Lyon, 1998.